Tellurium-Assisted Epitaxial Growth of Large-Area, Highly Crystalline ReS_2 Atomic Layers on Mica Substrate

Fangfang Cui, Cong Wang, Xiaobo Li, Gang Wang, Kaiqiang Liu, Zhou Yang, Qingliang Feng, Xing Liang, Zhongyue Zhang, Shengzhong Liu, Zhibin Lei, Zonghuai Liu, Hua Xu, and Jin Zhang**

2D transition metal dichalcogenides (TMDs) have been attracting increasing interests due to their unique structures and remarkable properties, which make them promising materials for a wide range of applications related to electronics, optoeletronics, valleytronics, spintronics, and catalysis.[1–5] As a member of the TMDs family, rhenium disulfide (ReS_2) possesses many distinctive features due to its unusual structure.[6] ReS_2 usually crystallizes in distorted octahedral (1T) crystal structure with triclinic symmetry.[7] The rhenium atoms within a monolayer form clusters of four Re atoms, which interlink together in diamond-shaped-chains (DS-chains) and give rise to the considerable anisotropy in electrical and optical properties.[8,9] The unusual anisotropic properties of ReS_2, similar to that of black phosphorus,[10,11] endow it with great potential for future novel device applications.[12] Furthermore, unlike WS_2 and MoS_2, the ReS_2 layers are charge decoupled from one another due to the Peierls distortion in the 1T structure of ReS_2 preventing ordered stacking and minimizes the interlayer overlap of wavefunctions.[6] As a result, from bulk to monolayer, ReS_2 remains a direct band gap semiconductor (1.5–1.6 eV).[13] Recently, few layer ReS_2 sheets with optical and electrical behavior different from group VI TMDs have been demonstrated to operate as field effect transistors,[13,14] digital inverters,[12] and photodetectors.[15]

F. F. Cui, C. Wang, X. B. Li, Dr. Z. Yang, Dr. X. Liang, Prof. S. Z. Liu, Prof. Z. B. Lei, Prof. Z. H. Liu, Prof. H. Xu
School of Materials Science and Engineering
Shaanxi Normal University
Xi'an 710119, P. R. China
E-mail: xuhua-nano@snnu.edu.cn

G. Wang, Prof. Z. Y. Zhang
School of Physics and Information Technology
Shaanxi Normal University
Xi'an 710119, P. R. China

Prof. K. Q. Liu
School of Chemistry and Chemical Engineering
Shaanxi Normal University
Xi'an 710119, P. R. China

Dr. Q. L. Feng, Prof. J. Zhang
Center for Nanochemistry
Beijing National Laboratory for Molecular Sciences
Key Laboratory for the Physics and Chemistry of Nanodevices
State Key Laboratory for Structural Chemistry of Unstable and Stable Species
College of Chemistry and Molecular Engineering
Peking University
Beijing 100871, P. R. China
E-mail: jinzhang@pku.edu.cn

DOI: 10.1002/adma.201600722

Previously, 2D ReS_2 has only been prepared by mechanical exfoliation from bulk crystal which was synthesized via chemical vapor transport at high temperature (>1000 °C) for several weeks.[16] Most recently, two groups have reported the synthesis of ReS_2 by using chemical vapor deposition (CVD) growth method, where ammonium perrhenate (NH_4ReO_4) and Re powder were used as Re source, respectively.[17,18] Though great efforts have been made to prepare 2D ReS_2, controllable synthesis of ReS_2 with high-crystal-quality and uniform thickness still faces great challenge. For example, using NH_4ReO_4 as Re source, which has high valence state Re (+7), to grow ReS_2 may suffer from low crystal quality due to lots of by-product.[18] Directly using Re powder as Re source can avoid this problem, but the high-melting point of Re (3180 °C) always lead to the low yield of ReS_2 because the low vapor pressure of Re inevitably restricts the vapor pressure of ReS_2 in the CVD system. Besides, the distorted 1T structure and the weaker interlayer coupling of ReS_2 make it preferable to grow into dendritic structure and thick flake on amorphous SiO_2 substrate.[17,18] These limitations pose great difficulty to the preparation of ReS_2, and thus restrict its application.

In this work, we demonstrate a tellurium-assisted CVD method to synthesize high quality monolayer ReS_2 in large-scale on mica substrate (**Figure 1**a,b). The idea is based on the Re–Te binary eutectic, whose eutectic point can be lowered down to 850 °C, even to 430 °C when Te–Re weight ratio is up to 90% (Figure S1, Supporting Information).[19] Hence, introducing Te powder into Re powder in growth system can greatly lower the originally high melting point of Re, and thus allows Re to volatilize into vapor phase at much lower growth temperature. Consequently, a vapor–vapor reaction between S and Re was realized, which dramatically increases the vapor pressure of ReS_2 in CVD growth system, and thus increases its growth efficiency. With this approach, large-area, highly crystalline ReS_2 can be synthesized in temperature range of 460–900 °C in atmospheric pressure. In addition, mica substrate, whose flat and inert surface favors the epitaxial growth, is critical to grow ReS_2 with uniform monolayer thickness. The morphology evolution of ReS_2 with growth temperature indicates that the off-symmetry growth tends to occur at higher growth temperature. The ReS_2 field-effect transistors (FETs) display n-type behavior with room temperature mobility of 4.1 $cm^2\ V^{-1}\ s^{-1}$ and current on/off ratio of 10^6. Angle-resolved polarized Raman spectroscopy and angle-dependent electrical measurements demonstrate superior anisotropic optical and electrical properties of the CVD-grown ReS_2. Our work not only promotes the large-scale application of ReS_2 in high performance electronic and

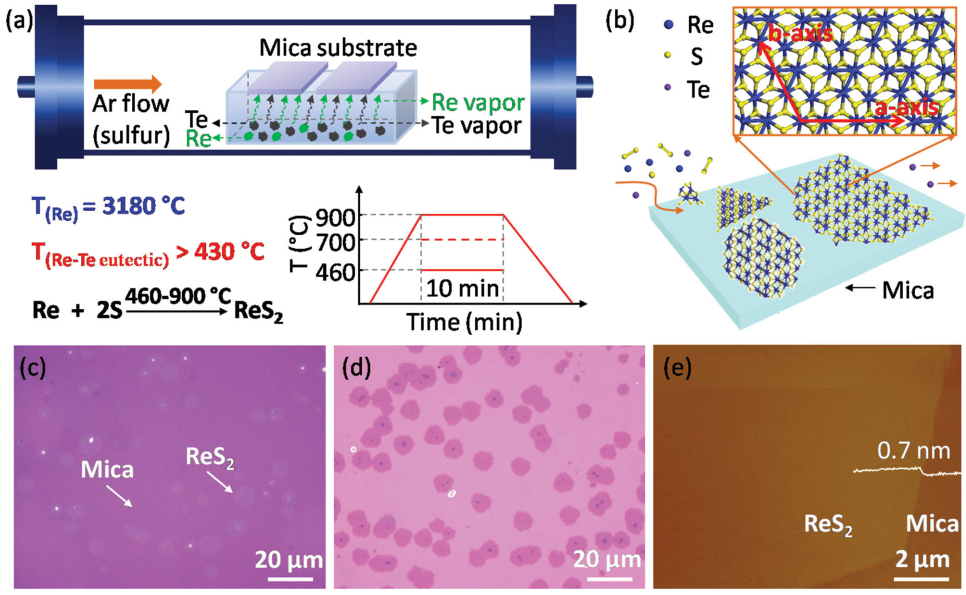

Figure 1. Schematic for a) the tellurium-assisted CVD growth approach and b) the surface reaction during epitaxial growth process of ReS_2 atomic layer on mica. Optical images of monolayer ReS_2 grown on c) mica substrate, d) after transferred onto SiO_2/Si (300 nm) substrate. e) AFM image of as-grown ReS_2 on mica substrate.

optoelectronic devices, but also helps us to understand the growth mechanism of the anisotropic materials.

Van der Waals (vdW) epitaxy is a powerful technique for the growth of high-crystalline-quality nanostructures from various compounds onto a substrate without surface dangling bonds, regardless of their lattice mismatch. In particular, a lot of quasi-2D layered structures with van der Waals gaps were successfully synthesized using this universal epitaxy technology.[20–22] The layered ReS_2 has a triclinic crystal structure in the space group (P-1), and each layer is held together by weak van der Waals interactions. Fluorophlogopite mica ($KMg_3AlSi_3O_{10}F_2$) is considered to be an excellent vdW epitaxy substrate for growing 2D materials, because of its atomic flatness, surface inertness, and rather high thermal stability.[20,23,24] The chemically inert substrate can circumvent strict requirement of lattice matching, facilitating the epitaxial growth of large-area, high-quality ReS_2 films.

The synthesis strategy of ReS_2 is schematically illustrated in Figure 1a. Briefly, Re powder and Te powder were mixed together with weight ratio of 1:6, and placed into ceramic boat in the hot center inside the tube furnace. Sulfur powder was placed near the outside edge of the hot zone, where the temperature is ≈200 °C. Freshly cleaved fluorophlogopite mica substrates were put onto the ceramic boat. Typical growth conditions were carrier gas (Ar) flow rate of 80 sccm, growth temperature of 700 °C and growth time of 10 min. Figure 1c,d shows the typical optical microscopy (OM) image of an as-grown ReS_2 on mica substrate and transferred onto SiO_2/Si substrate, respectively. We can see that large-scale ReS_2 flakes and even continuous ReS_2 film (Figure S2, Supporting Information) with uniform thickness were obtained. The results show great difference compared to that grown from only Re powder and S powder precursors, where just a few ReS_2 flakes scattered on the SiO_2/Si substrate (Figure S3a,b, Supporting Information), indicating the high growth efficiency of ReS_2 by using our tellurium-assisted CVD growth method. The high growth efficiency is attributed to the low melting point of the forming Te–Re binary eutectic, which greatly decreases the growth temperature, while increases the vapor pressure of ReS_2 in the CVD system.

Atomic force microscopy (AFM) image reveals that the ReS_2 has a thickness of ≈0.7 nm, demonstrating a monolayer. In addition, the ReS_2 surface has a roughness of ≈0.1 nm, which is similar to that of the mica substrate, indicating high quality epitaxial growth of this material. In contrast, thick flakes and flower-like structure ReS_2 tend to grow on amorphous SiO_2 substrate (Figure S3c,d, Supporting Information). Unlike other TMDs, the weak interlayer coupling of ReS_2 make the Frank–van der Merwe growth (layer-by-layer growth) occur much too easy, and thus ReS_2 prefer to grow into thick flakes on usual substrate. The apparent thickness and morphological difference between products on mica and that on SiO_2 originate from the variation of migration barrier energy (E_m). The E_m of adatoms on SiO_2 surface is much bigger than that on mica because of the stronger interaction between adatoms and SiO_2 substrate which has a large amount of unsaturated dangling bands.[25] Considering the migration coefficient D is related to E_m by

$$D \propto e^{-E_m/kT} \quad (1)$$

where k is the Boltzmann constant and T is the substrate temperature.[25] The migration coefficient on SiO_2 surface is far lower than that on mica with the same growth temperature and time. Therefore, the atomically flat surface of mica facilitates precursor migration during CVD growth, thereby improving the thickness uniformity of resulting ReS_2 layer. Moreover, bilayer, few layer, and thick flakes can also be obtained (Figure S4, Supporting Information) when grown at higher growth temperature (>800 °C).

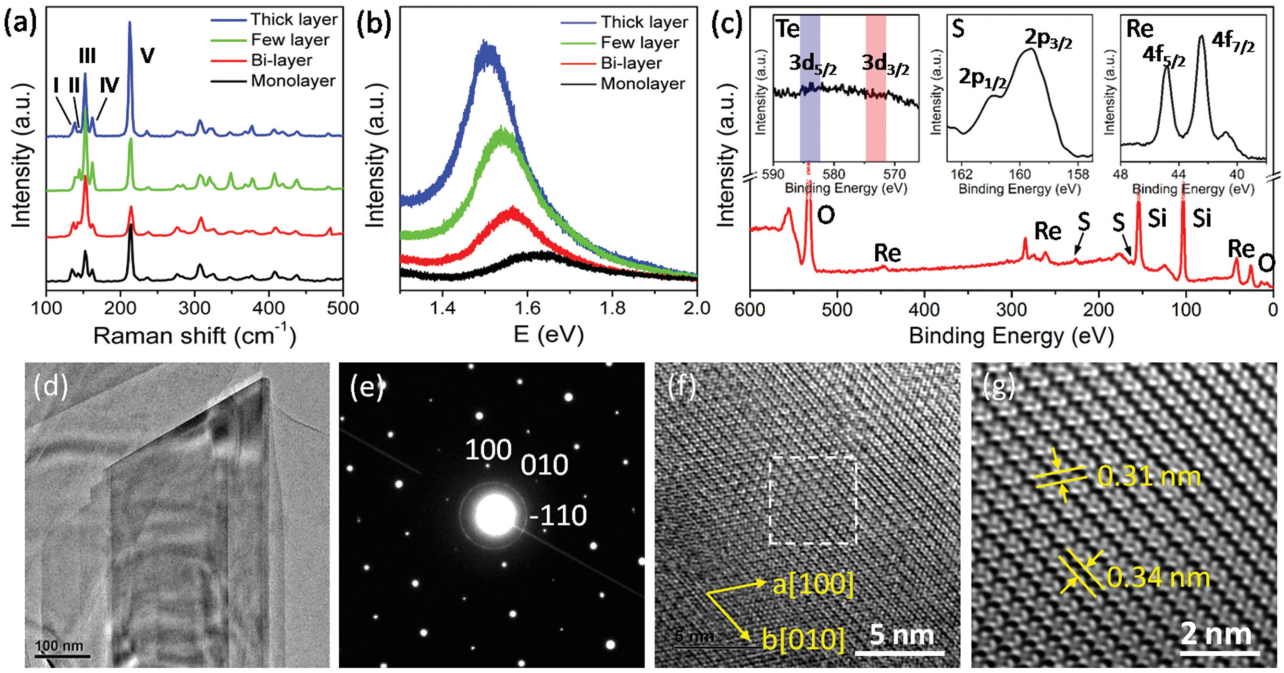

Figure 2. Structure and composition characterization of CVD-grown ReS_2. a) Raman and b) fluorescence spectra of ReS_2 with thickness varying from monolayer to thick layer. c) Full XPS spectra of $ReS_2$with insets for the Re 4f spectrum, S 2p spectrum, and Te 3d spectrum. d) Low-resolution TEM image of the ReS_2 supported on a TEM grid. e) SAED patterns of the ReS_2. f) High-resolution TEM image of the ReS_2. g) Fast Fourier-transform (FFT) image of the marked area in (f).

Raman spectra of monolayer, bilayer, few layer, and thick platelets (≈30 nm) were collected with a 532 nm excitation laser (**Figure 2**a). The typical phonon vibration modes can be identified from the Raman spectra in the range of 100–500 cm^{-1}, which matches well with the mechanically exfoliated samples. The main Raman peaks at ≈162 and ≈213 cm^{-1} correspond to the in-plane (IV) and out-of-plane (V) vibrational modes, respectively. A series of additional Raman modes in the range of 100–500 cm^{-1} arise due to symmetry splitting in the distorted 1T structure. Notably, there are no Raman peaks at ≈120 cm^{-1}, corresponding to the A_1 mode of elemental Te (Figure S5, Supporting Information), was observed in these Raman spectra proving no Te precipitates in our grown ReS_2 sample. Similar to previous work,[9] the Raman spectra show a slightly sensitive to the layer number due to the interlayer decoupling of ReS_2 (Figure S6, Supporting Information). In addition, ReS_2 samples with different thickness exhibit obvious photoluminescence (PL) emission at room temperature (Figure 2b). From bulk to monolayer, the peak energy increases slightly from 1.5 to 1.6 eV, while the PL intensity decreases, which are attributed to the direct band gap and interlayer decoupling properties of ReS_2. All these spectrum features of the CVD-grown ReS_2 exhibit stark contrast to the behavior observed in conventional TMDs such as MoS_2, $MoSe_2$, WS_2, and WSe_2.[6,13,26] Furthermore, the strong optical anisotropic properties of the CVD-grown ReS_2 were revealed by using angle-resolved polarized Raman spectra (Figure S7, Supporting Information), which can be used to identify the crystal orientation of ReS_2.

X-ray photoelectron spectroscopy (XPS) was utilized to examine the elemental composition and bonding types in the CVD-grown ReS_2. Re and S were seen from the survey spectra of the CVD-grown films along with Si and O from the Si/SiO_2 substrate (Figure 2c). The prominent $4f_{7/2}$ and $4f_{5/2}$ level peaks for Rhenium are located at ≈42.5 and ≈44.8 eV, respectively. The prominent $2p_{3/2}$ and $2p_{1/2}$ level peaks for sulfur are located at ≈159.7 and ≈160.9 eV, respectively. These features are consistent with the XPS spectra of exfoliated bulk ReS_2 crystal.[14] Additionally, the atomic ratio between Re and S elements is 1:1.98, indicating that the CVD-grown ReS_2 is stoichiometric. It is noteworthy that the prominent $3d_{5/2}$ and $3d_{3/2}$ peaks for tellurium, located at ≈573 and ≈583.4 eV, are not observed, indicating the absence of Te in the crystal structure of ReS_2. This is reasonable, because the extreme weak oxidability of Te make the reaction between Re and Te very difficult, or almost impossible, especially under the S rich atmosphere. The volatile Te is carried outside the reaction system along with carrier gas during growth process. Therefore, the additive Te does not create destruction to the crystal structure of ReS_2, while it acts as a transfer agent to bring solid Re into vapor phase to promote the growth efficiency of ReS_2.

The crystallographic structure of CVD-grown ReS_2 was further characterized by high-resolution transmission electron microscopy (HRTEM) and selected area electron diffraction (SAED). Figure 2d shows a lower magnification transmission electron microscopy (TEM) image of our ReS_2 film. The continuity of the film suggests that our ReS_2 is of high quality. HRTEM image shows the well crystal structure without defect, and the DS-chains in the b direction are clearly visible (Figure 2f). The angle between b[010] and a[100] axes is ≈59.9° (Figure 2e), and the lattice spacing between two vicinal DS-chains in the direction of b and a are 0.34 and 0.31 nm for ReS_2 (Figure 2g), which are consistent well with the structure of exfoliated ReS_2.[8]

Based on the Re–Te binary-phase diagram, ReS_2 film can be grown at any temperature above 430 °C as shown in Figure S8 (Supporting Information). The morphology of ReS_2 grown at different temperatures show obvious variation (**Figure 3**), changing from round at 500 °C to hexagon at 600 °C, and then to serration at 700 °C, finally to dendritic structure at 850 °C. The dendritic morphology of ReS_2 indicates the off-symmetry growth of this material, which is attributed to the distorted 1T structure induced anisotropic interfacial energy.[17] The temperature-modulated morphology evolution indicates that the off-symmetry growth tends to occur at higher growth temperature (>700 °C). This phenomenon can be understood from the temperature dependent migration coefficient of adatoms on substrate as shown in Equation (2). At low temperature, the slow atomic diffusion and the unfree attachment and detachment of adatoms at ReS_2 edge allow the epitaxial growth occur at different crystal axis directions with nearly the same rate. So, we can see in Figure 1d most nanoplates are round shapes. At high temperature, the atomic diffusion becomes fast, and the adatoms tend to migrate and attach to the high-activation growth direction [010] where energetically favorable. As a result, the off-symmetry growth of the anisotropic ReS_2 becomes apparent at high growth temperature. Furthermore, Raman spectra of ReS_2 grown at different temperature indicate that high quality ReS_2 can be obtained when grown above 600 °C (Figure 3i). Therefore, the growth temperature plays an important role in the morphology and crystal quality control of ReS_2 growth.

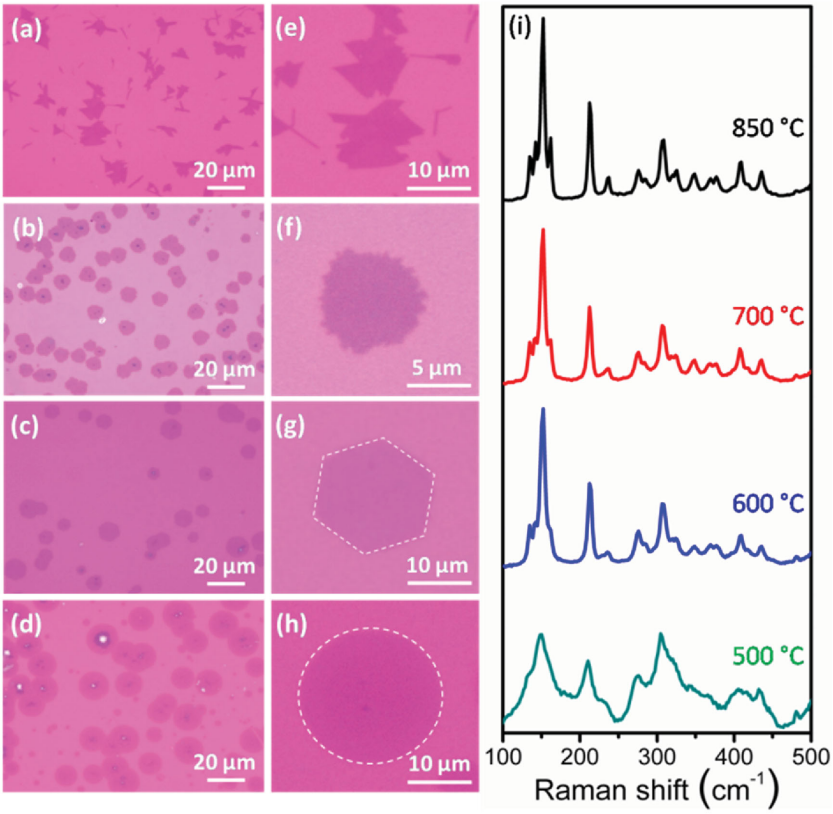

Figure 3. Temperature-dependent growth behavior of ReS_2. a–d) OM images of ReS_2 grown at 850, 700, 600, 500 °C after transferred on SiO_2/Si substrate. e–h) Corresponding enlarged images. i) Raman spectra of ReS_2 grown at different temperatures.

Transport measurements were used to characterize the electrical properties of our CVD-grown ReS_2 film. **Figure 4**a shows the OM image of a typical ReS_2 FET device. The linear I_{ds}–V_{ds} characteristic suggests that ohmic contacts are formed between the Cr/Au metal pads and ReS_2 (Figure 4b). The ReS_2 device exhibits n-type conduction with a current on/off ratio up to 10^6 and a threshold voltage of –28 V (Figure 4d). Based on the equation for the carrier mobility

$$\mu = \frac{L}{WV_{ds}C_g} \cdot \frac{dI_{ds}}{dV_{bg}} \quad (2)$$

where L, W, and C_g stand for the channel length, width, and the gate capacitance per unit area, respectively, the field-effect electron mobility of this ReS_2 FET is calculated to be 1.43 $cm^2\ V^{-1}\ s^{-1}$. Furthermore, direction-dependent electrical measurement shows the conductance and mobility parallel to the DS-chains (b direction) are 0.11 μS and 4.01 $cm^2\ V^{-1}\ s^{-1}$, respectively, while that perpendicular to the DS-chains are lower, being 0.025 μS and 1.32 $cm^2\ V^{-1}\ s^{-1}$, respectively (Figure 4e,f). The mobility of our ReS_2 is even comparable with that of mechanically exfoliated ReS_2 flakes (1–15 $cm^2\ V^{-1}\ s^{-1}$),[12,14] and the ratio of conductance and mobility along two principle axes reaches 4.4:1 and 3:1, respectively. These results confirm the high crystal quality and large in-plane anisotropic properties of CVD-grown ReS_2.

In summary, based on tellurium-assisted volatilization of Re gas, we present an effective CVD growth technique to produce large-scale, highly crystalline ReS_2 atomic layers. The distorted 1T structure induced off-symmetry growth of ReS_2 becomes apparent at higher growth temperature. The electrical transport properties of our ReS_2 are comparable with those of mechanically exfoliated ReS_2 flakes, and exhibit stronger anisotropy. The high crystallinity and superior anisotropy of ReS_2, combined with controllable growth make it promising 2D materials for future electronics and new concept devices applications.

Experimental Section

Monolayer ReS_2 Epitaxial Growth and Transfer: Large-area monolayer ReS_2 was grown in a single temperature-zone tubular furnace (Lindberg/Blue M) equipped with a 1 in. diameter quartz tube under atmospheric pressure. Sulfur powder (purity 99.5%) was placed near the outside edge of the hot zone, where the temperature is ≈200 °C. Re powder (purity 99.99%) and Te power (purity 99.9%) were mixed together with weight ratio of 1:6, and placed into ceramic boat in the hot center inside the tube furnace. Freshly cleaved fluorophlogopite

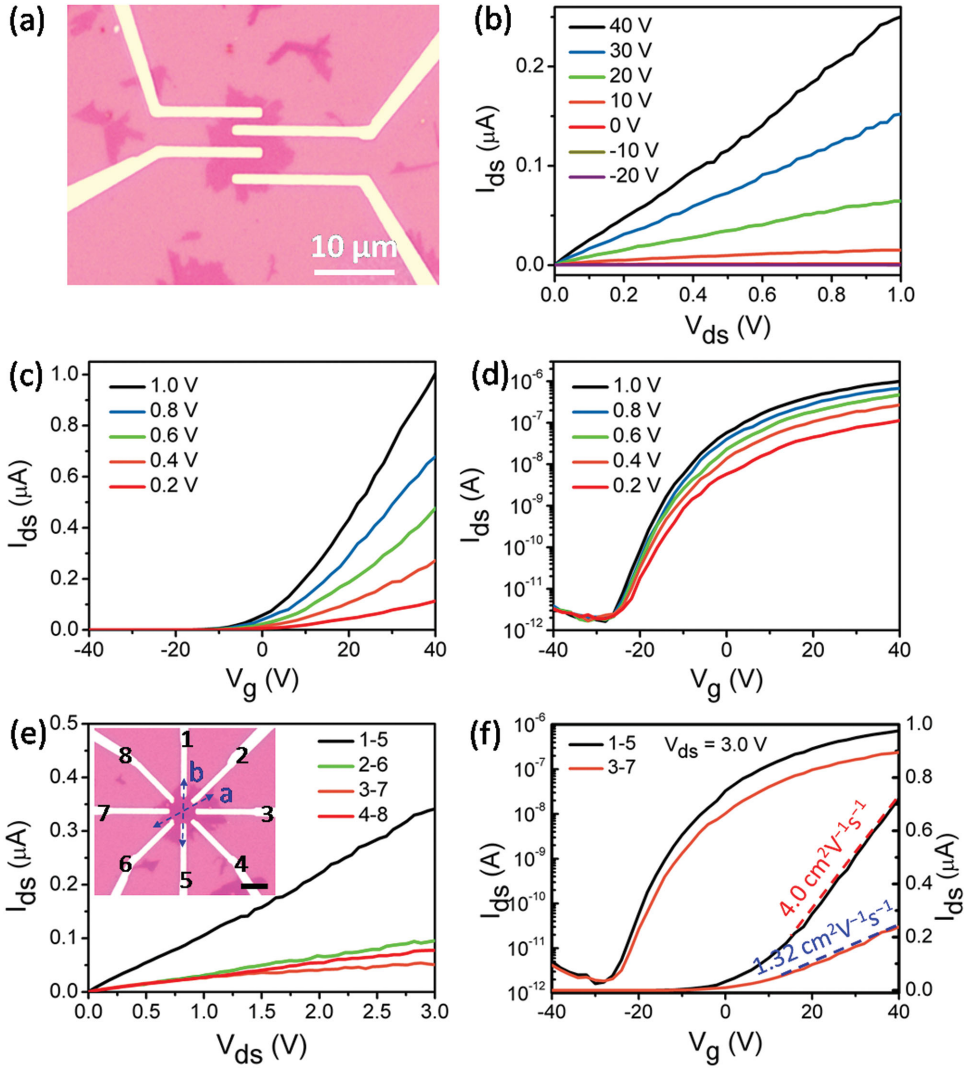

Figure 4. Electrical properties of devices made from a monolayer ReS_2. a) A typical OM image of a ReS_2 device on 300 nm SiO_2/Si. b) Source-drain current (I_{ds}) versus voltage (V_{ds}) characteristics of our ReS_2 FET device at various values of gate voltage. c,d) Source-drain current (I_{ds}) versus gate voltage curve for the same devices at various values of V_{ds} on a linear scale (c) and a logarithmic scale (d), respectively. Angle-dependent (e) transfer curves (V_{ds} = 3.0 V) and f) *I–V* curves (V_g = 40 V).

mica substrates were put onto the ceramic boat. Typical growth conditions were carrier gas (Ar) flow rate of 80 sccm, growth temperature of 700 °C, and growth time of 10 min. Subsequently, the as-grown ReS_2 sample was transferred onto SiO_2/Si (300 nm) substrate with the aid of poly (methyl methacrylate) by using a portable transfer method. Hydrofluoric acid (20 wt%) was used as the etchant to delaminate ReS_2 monolayer from mica substrate.

Characterizations of Epitaxial Monolayer ReS_2: The prepared samples were systematically characterized using optical microscopy (Olympus BX51), Raman spectroscopy (Renishaw), AFM (Bruker Dimension ICON) and TEM (Tecnai G2 F20; acceleration voltage, 200 kV). A lacey carbon film supported on copper grids was used for TEM characterization, onto which ReS_2 layer was transferred with similar method described in the last paragraph. For angle-resolved polarized Raman experiments, a polarizer was placed in the incident laser path to obtain the *x*-direction polarized light, and polarized Raman spectra with different angle θ were obtained by rotating the ReS_2 sample.

Device Fabrication and Electrical Measurement: ReS_2 sample was transferred onto SiO_2/Si (300 nm) substrate. Electrical contacts with ReS_2 sample were achieved using standard electron beam lithography and thermal evaporation of 5 nm Cr and 50 nm Au. Electrical transport properties were measured in ambient air conditions using an Agilent B2912A source-meter unit.

Supporting Information

Supporting Information is available from the Wiley Online Library or from the author.

Acknowledgements

F.F.C., C.W., and X.B.L. contributed equally to this work. The authors acknowledge the insightful suggestions and comments from Dr. S. C. Zhang, N. N. Mao, and J. X. Wu at Peking University. This work was supported by the National Natural Science Foundation of China

(Grant No. 51222201), and the fundamental Research Funds for the Central Universities (GK201502003).

Received: February 5, 2016
Revised: February 28, 2016
Published online: April 28, 2016

[1] R. Cheng, S. Jiang, Y. Chen, Y. Liu, N. Weiss, H. C. Cheng, H. Wu, Y. Huang, X. F. Duan, *Nat. Commun.* **2014**, *5*, 5143.
[2] Q. H. Wang, K. Kalantar-Zadeh, A. Kis, J. N. Coleman, M. S. Strano, *Nat. Nanotechnol.* **2012**, *7*, 699.
[3] H. L. Zeng, J. F. Dai, W. Yao, D. Xiao, X. D. Cui, *Nat. Nanotechnol.* **2012**, *7*, 490.
[4] X. D. Xu, W. Yao, D. Xiao, T. F. Heinz, *Nat. Phys.* **2014**, *10*, 343.
[5] Y. F. Yu, S. Y. Huang, Y. P. Li, S. N. Steinmann, W. T. Yang, L. Y. Cao, *Nano Lett.* **2014**, *14*, 553.
[6] S. Tongay, H. Sahin, C. Ko, A. Luce, W. Fan, K. Liu, J. Zhou, Y. S. Huang, C. H. Ho, J. Y. Yan, D. F. Ogletree, S. Aloni, J. Ji, S. S. Li, J. Li, F. M. Peeters, J. Q. Wu, *Nat. Commun.* **2014**, *5*, 3252.
[7] C. H. Ho, *Opt. Express* **2005**, *13*, 8.
[8] Y. C. Lin, H. P. Komsa, C. H. Yeh, T. Björkman, Z. Y. Liang, C. H. Ho, Y. S. Huang, P. W. Chiu, A. V. Krasheninnikov, K. Suenaga, *ACS Nano* **2015**, *9*, 11249.
[9] D. A. Chenet, O. B. Aslan, P. Y. Huang, C. Fan, A. M. van der Zande, T. F. Heinz, J. C. Hone, *Nano Lett.* **2015**, *15*, 5667.
[10] F. N. Xia, H. Wang, Y. C. Jia, *Nat. Commun.* **2014**, *5*, 4458.
[11] J. X. Wu, N. N. Mao, L. M. Xie, H. Xu, J. Zhang, *Angew. Chem. Int. Ed.* **2015**, *54*, 2366.
[12] E. F. Liu, Y. J. Fu, Y. J. Wang, Y. Q. Feng, H. M. Liu, X. G. Wan, W. Zhou, B. G. Wang, L. B. Shao, C. H. Ho, Y. S. Huang, Z. Y. Cao, L. G. Wang, A. D. Li, J. W. Zeng, F. Q. Song, X. R. Wang, Y. Shi, H. T. Yuan, H. Y. Hwang, Y. Cui, F. Miao, D. Y. Xing, *Nat. Commun.* **2015**, *6*, 6991.
[13] E. Zhang, Y. B. Jin, X. Yuan, W. Y. Wang, C. Zhang, L. Tang, S. S. Liu, P. Zhou, W. D. Hu, F. X. Xiu, *Adv. Funct. Mater.* **2015**, *25*, 4076.
[14] C. M. Corbet, C. McClellan, A. Rai, S. S. Sonde, E. Tutuc, S. K. Banerjee, *ACS Nano* **2015**, *9*, 363.
[15] F. C. Liu, S. J. Zheng, X. X. He, A. Chaturvedi, J. F. He, W. L. Chow, T. R. Mion, X. L. Wang, J. D. Zhou, Q. D. Fu, H. J. Fan, B. K. Tay, L. Song, R. H. He, C. Kloc, P. M. Ajayan, Z. Liu, *Adv. Funct. Mater.* **2016**, *26*, 1147.
[16] C. H. Ho, Y. S. Huang, K. K. Tiong, P. C. Liao, *J. Phys.: Condens. Matter* **1999**, *11*, 5367.
[17] K. Keyshar, Y. J. Gong, G. Ye, G. Brunetto, W. Zhou, D. P. Cole, K. Hackenberg, Y. He, L. Machado, M. Kabbani, A. H. C. Hart, B. Li, D. S. Galvao, A. George, R. Vajtai, C. S. Tiwary, P. M. Ajayan, *Adv. Mater.* **2015**, *27*, 4640.
[18] X. X. He, F. C. Liu, P. Hu, W. Fu, X. L. Wang, Q. S. Zeng, W. Zhao, Z. Liu, *Small* **2015**, *11*, 5423.
[19] T. K. Kurbanov, R. A. Dovlyatshina, I. A. Dzhavodova, F. A. Akhmenov, *Russ. J. Inorg. Chem.* **1977**, *22*, 622.
[20] H. Li, J. Cao, W. S. Zheng, Y. L. Chen, D. Wu, W. H. Dang, K. Wang, H. L. Peng, Z. F. Liu, *J. Am. Chem. Soc.* **2012**, *134*, 6132.
[21] Y. M. Shi, W. Zhou, A. Y. Lu, W. J. Fang, Y. H. Lee, A. L. Hsu, S. M. Kim, K. K. Kim, H. Y. Yang, L. J. Li, J. C. Idrobo, J. Kong, *Nano Lett.* **2012**, *12*, 2784.
[22] W. H. Dang, H. L. Peng, H. Li, P. Wang, Z. F. Liu, *Nano Lett.* **2010**, *10*, 2870.
[23] Q. Q. Ji, Y. F. Zhang, T. Gao, Y. Zhang, D. L. Ma, M. X. Liu, Y. B. Chen, X. F. Qiao, P. H. Tan, M. Kan, J. Feng, Q. Sun, Z. F. Liu, *Nano Lett.* **2013**, *13*, 3870.
[24] H. L. Peng, W. H. Dang, J. Cao, Y. L. Chen, D. Wu, W. S. Zheng, H. Li, Z. X. Shen, Z. F. Liu, *Nat. Chem.* **2012**, *4*, 281.
[25] Q. S. Wang, K. Xu, Z. X. Wang, F. Wang, Y. Huang, M. Safdar, X. Y. Zhan, F. M. Wang, Z. Z. Cheng, J. He, *Nano Lett.* **2015**, *15*, 1183.
[26] A. Splendiani, L. Sun, Y. Zhang, T. Li, J. Kim, C. Y. Chim, G. Galli, F. Wang, *Nano Lett.* **2010**, *10*, 1271.